ACS Sustainable Chemistry & Engineering

pubs.acs.org/journal/ascecg

Research Article

A Transparent, Degradable Polymer Electrode Inspired by Skeleton Flowers for Versatile Transient Electronics

Chuanfeng Wang,[▽] Chu Pan,[▽] Zhu Liu, Liang Lu, Yu Lai, Juan Li, Zhipei Xia, Weiqing Yang,* and Jun Lu*

Cite This: *ACS Sustainable Chem. Eng.* 2026, 14, 198−208

Read Online

ACCESS | Metrics & More | Article Recommendations | Supporting Information

ABSTRACT: Transparent, degradable electrodes are essential for the development of versatile, degradable electronics. Yet, the use of crystalline degradable polymers as transparent electrode materials remains a huge challenge due to the inability to break the trade-off between light transmittance, electrical conductivity, and mechanical strength. Here, inspired by skeleton flowers, we develop a microbial polyhydroxybutyrate (PHB)-based transparent material with a fibrous structure by combining electrospinning and high-pressure crystallization. High pressure reduces the air−fiber interface, induces preferential crystal orientation, and thus enhances the transparency of highly crystalline, nanofibrous-structured PHB materials. Sequentially, we construct a silver nanowire (AgNW) network on the transparent fibrous PHB substrate and produce a transparent, conductive AgNW/PHB-based film that combines good electrical conductivity, high light transmittance, and robust mechanical performance. The AgNW/PHB-based film demonstrates great potential for applications in versatile transient electronic devices. It can serve as an eco-friendly transparent degradable electrode in biobased piezoelectric nanogenerators. This innovation allows for the first creation of a fully degradable, environmentally friendly, luminescent, and self-powered flexible bioelectric device. We postulate that this work opens up new possibilities for further advancements in transient electronics.



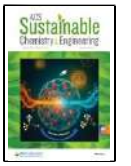
KEYWORDS: *Degradable electronics, Transparent electrode, Electrospinning, High pressure, Piezoelectric nanogenerator (PENG), Polyhydroxybutyrate (PHB)*

INTRODUCTION

Electronic wastes do cause much harm to the environment and health.[1−4] Consequently, transient electric devices have attracted much attention and are a hot spot.[5−17] The degradable electrode is an important component of transient electronics.[5,10,14,16] Transparent electronics is an important branch of electronics[17,18] and widely used in household appliances,[19] portable equipment,[20,21] architecture,[22] medicine,[23] national defense,[24] etc. It includes the development and application of transparent electrodes.[25−27] These electrodes play an important role in collecting charge, transmitting signals, or ensuring that devices achieve specific functions.[25−29] Consequently, the transparent electrode is one of the important contents of transparent electronics.[25,30,31] However, most transparent electrodes lack degradability. At present, the preparation approaches of transparent electrodes include thermal evaporation,[32,33] magnetron sputtering,[34,35] sol−gel[36,37] and spray methods,[38,39] etc. Most of these methods are complex or costly or harm to the environment. Therefore, the transparent degradable electrode (TDE) and the simple, environmentally friendly method are valuable and necessary and are beneficial for the advancement of transient electronics.[40−44] TDE can be used in traditional electronics[45] and plays an important role in medicine,[46,47] wearable electronics,[40,41] photovoltaic cells,[42,48] etc. Nonetheless, there are many challenges in TDE, such as degradability, optical properties and conductivity, preparation technology and cost, etc.[49−51] Especially, the selection of the material and the preparation method have an important influence on the performance of TDE.

Recent studies have revealed interesting progress in the development of composite conductors by combining matrix materials with conductive materials.[52−54] For example, Juang et al. reported the first fabrication of silver nanowire (AgNW)/gallium-doped ZnO (GZO) composite transparent conductive electrodes (TCEs) on ultrathin flexible glass substrates using an atmospheric pressure plasma jet (APPJ) system.[52,53]

Received: August 29, 2025
Revised: December 7, 2025
Accepted: December 8, 2025
Published: December 25, 2025



Downloaded from pubs.acs.org/ascecg/article-pdf/14/1/198/6380243/sc5c09169.pdf by SOUTHWEST JIAOTONG UNIV user on 07 November 2026

© 2025 American Chemical Society

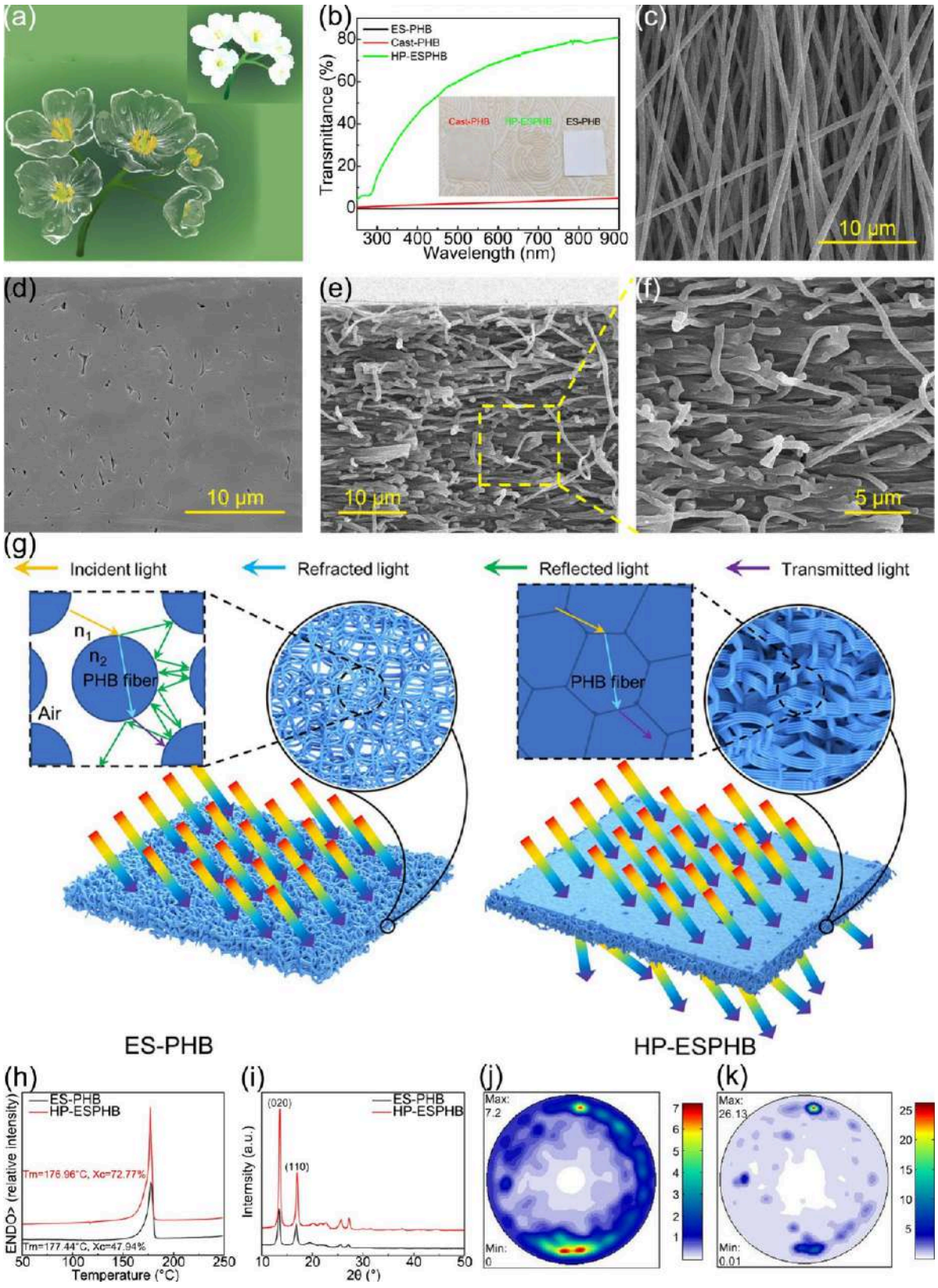


Figure 1. (a) Appearances of *Diphylleia grayi* before rain (upper right) and after rain (lower left). (b) Transparency of PHB films prepared by different methods. The inset shows the digital picture of ES-PHB, Cast-PHB, and HP-ESPHB films. The thickness of the films is ∼70 μm. (c) SEM of ES-PHB fibers. (d−f) SEM of the surface (d) and cross sections (e, f) of the HP-ESPHB film. (g) Schematic illustration of the light transmittance mechanism of ES-PHB and HP-ESPHB. DSC (h) and WAXD (i) of ES-PHB and HP-ESPHB. (j, k) XRD pole figures of the (020) crystal plane of ES-PHB (j) and HP-ESPHB (k).

https://doi.org/10.1021/acssuschemeng.5c09169
ACS Sustainable Chem. Eng. 2026, 14, 198−208

Downloaded from pubs.acs.org/ascecg/article-pdf/14/1/198/6380243/sc5c09169.pdf by SOUTHWEST JIAOTONG UNIV user on 07 November 2026

Moreover, Shi and co-workers proposed a semiwrapped structure based on silver nanowires (AgNWs) and water-soluble poly(vinyl alcohol) (PVA) and developed a recyclable, stable strain sensor using the semiwrapped AgNWs/PVA-based composite conductive film.[54]

Polyhydroxybutyrate (PHB) is a crystalline chiral polyester synthesized by microbial fermentation.[55−59] It has reproducibility, biocompatibility, and degradability.[55,56,58] However, PHB products have poor light transmittance and high brittleness.[60−62] Crystalline degradable polymers are composed of both crystalline and amorphous phases.[56,62,63] In comparison to amorphous degradable polymers, the presence of crystalline regions in these crystalline degradable polymers enhances mechanical strength but reduces light transmittance.[56,62,63] Besides this, the high conductivity of polymer-based electrodes is usually at the expense of optical transmittance.[48,51] Therefore, the use of crystalline degradable polymers as transparent electrode materials has been highly challenging due to the inability to break the trade-off between light transmittance, electrical conductivity, and mechanical strength.

Diphylleia grayi, also known as the skeleton flower, is an interesting plant. It becomes transparent when exposed to water (Figure 1a). After water droplets come into contact with the petals of *Diphylleia grayi*, they gradually infiltrate the space in the petals. As the refractive index of water and cell sap is close, the reflection interface is eliminated, and the light transmittance of the petals is hence improved. Inspired by this plant, first, we carried out high-pressure treatment to electrospun PHB (ES-PHB) film at an appropriate temperature. This reduces the fiber−air interfaces and leads to crystal orientation, and a transparent fibrous film is thus obtained. Furthermore, a transparent and conductive AgNW/ESPHB-based composite film is fabricated. The composite film also has degradability and great mechanical properties and can be used as a TDE. This means that it has enormous value in degradable electronics.

EXPERIMENTAL SECTION

Materials. PHB was purchased from Tianan Co., Ltd., Ningbo, China. AgNW (10 mg/mL) was provided by Ouyi Organic Optoelectronic Material Co., Ltd., Shanghai, China. The aspect ratio was about 330 with a diameter of 30−60 nm and a length of 10−20 μm. Degradable packaging material (DPM) was acquired from Xing Chuangyi Technology Co., Ltd., Shenzhen, China. Dimethylformamide (DMF) was obtained by Haihong Instruments and Apparatus Co., Ltd., Chengdu, China. Chloroform was supplied by Kelong Co., Ltd., Chengdu, China. A commercial indium tin oxide-polyethylene terephthalate (ITO-PET) film, composed of a PET substrate and transparent ITO layer, was purchased from South China Xiangcheng Technology Co., Ltd., Yiyang, China.

Preparation of ES-PHB Film. The PHB was dissolved in a mixture of chloroform and DMF. The ratio of chloroform to DMF was 9:1 (v/v). The polymer solution had a concentration of approximately 0.07 g/mL. Afterward, the solution was transferred to a syringe. The syringe was securely attached to a pump and connected to a spinneret. The injection rate of the solution was set to 10 μL/min. A positive voltage of 11 kV was applied between the spinneret and the receiving equipment. In this setup, a metallic rotating roller served as the receiving terminal. The distance between the spinneret and the roller was maintained at 20 cm. Finally, the nanofiber mat was detached from the roller and stored in a plastic bag. The diameter distribution histogram of ES-PHB fibers is shown in Figure S1.

Preparation of Casting PHB (Cast-PHB) Film. A predetermined amount of PHB raw material was weighed and placed in a beaker. DMF was added to the beaker as a solvent. The mixture was heated in an oil bath at 131 °C for approximately 40 min to dissolve PHB in DMF. The resulting solution was poured into a Petri dish and transferred to an oven set at 80 °C to evaporate DMF. The solvent evaporation process lasted about 12 h. Finally, a freestanding PHB film was formed. No fibrous structure was observed in the Cast-PHB film (Figure S2a,b). Also, it was highly crystalline (Figure S2c).

Preparation of Transparent HP-ESPHB Film. As shown in Figure S3, the ES-PHB film was placed between two layers of PI. Then, a pressure of 200 MPa was applied at 140 °C for 60 min. After the device cooled, the high-pressure ES-PHB (HP-ESPHB) film was removed from the PI membrane.

The relationship between processing parameters (pressure, temperature, and holding time) and optical transmittance was investigated (Figure S4). The data indicated that increasing either temperature or pressure led to an improvement in the optical transmittance of the HP-ESPHB film. However, saturation behavior was observed. The extent of improvement diminished progressively at higher levels of temperature or pressure. In contrast, the holding time had a negligible effect on the light transmittance of the HP-ESPHB film.

Preparation of Transparent Conductive AgNW/ESPHB Film. As shown in Figure S5, the AgNW was dispersed on the ES-PHB film by filtration. Simultaneously, PHB fibers were deposited on a piece of PI membrane for 60 min by electrospinning. Then, the PI membrane covered with PHB fibers was superimposed on the ES-PHB film dispersed with AgNW. A pressure of 200 MPa was subsequently applied to the multilayer structure at 140 °C for 10 min. After the device was cooled, the conductive AgNW/ESPHB film was removed from the PI membrane. Table S1 and Figure S6 show the comparison of different environmentally friendly, degradable transparent conductive materials in terms of different aspects.

Characterization. The samples were coated with gold for observation under a JSM-IT500 scanning electron microscope (SEM). Energy dispersive spectroscopy (EDS) was conducted using an Oxford X-Max 80 spectrometer. A UV spectrophotometer (UV-3600) was employed to measure the light transmittance of the PHB-based films. Differential scanning calorimetry (DSC) was performed to characterize the crystallinity and molten behaviors of PHB-based samples using a DSC 2500 instrument. The crystallinity (X_c) was calculated with the following equation

$$X_c = \frac{\Delta H_m}{\Delta H_m^0} \quad (1)$$

where ΔH_m is the endothermic enthalpy of the molten peak of PHB crystals and ΔH_m^0, 146 J/g, is the equilibrium melting enthalpy of the ideal PHB crystal.[64] X-ray diffraction (XRD) spectra were obtained at atmospheric pressure using an Empyrean instrument. X-ray pole figures were measured using an Empyrean Series 2 diffraction system. A resistivity tester (RTS-9) was used to determine the surface resistance of the conductive AgNW/ESPHB-based fibrous films.

Fabrication of AgNW/ESPHB-Based Resistive Sensor. Two copper foils were connected to both ends of the AgNW/ESPHB film (Figure S7). They were used for the transmission of resistance signals. Then, the structure was encapsulated with a degradable packaging material (DPM).

Fabrication of Transient PENG. The green emissive, piezoelectric carbon quantum dot/cellulose nanocrystal/polyhydroxybutyrate (CQD/CNC/PHB)-based fibrous mats were used as the piezo-active layer of piezoelectric nanogenerator (PENG) devices (Figure S8). The fully biobased, transient PENG consisted of CQD/CNC/PHB-based fiber mats and AgNW/ESPHB-based films (Figure S9). The piezo-active CQD/CNC/PHB-based mats were sandwiched between two layers of AgNW/ESPHB films. The AgNW/ESPHB films were used as the transparent conductive electrodes of the transient PENG. For structural stability and protection, the entire assembly was encapsulated using the DPM.

Degradation of Transient PENG. The hydrolytic degradation of PENG was conducted in an alkali aqueous solution (pH 12) of

Downloaded from pubs.acs.org/ascecg/article-pdf/14/1/198/6380243/sc5c09169.pdf by SOUTHWEST JIAOTONG UNIV user on 07 November 2026

https://doi.org/10.1021/acssuschemeng.5c09169
ACS Sustainable Chem. Eng. 2026, 14, 198−208

sodium hydroxide at 58 °C. The composting decomposition of PENG was carried out in a well-fermented compost material at about 58 °C.

RESULTS AND DISCUSSION

As shown in Figure 1b, a transparency comparison of casting PHB (Cast-PHB) film, ES-PHB film, and high-pressure ES-PHB (HP-ESPHB) is conducted. Obviously, HP-ESPHB film has higher light transmittance. Figure 1c shows the morphology of the ES-PHB fiber before high-pressure treatment. Here, ES-PHB fibers have continuous fibrous structures and smooth fiber surfaces. Figure S1 exhibits the distribution of ES-PHB fibers diameter. Most of the PHB fibers have diameters ranging from 400 to 700 nm. The average fiber diameter is 574.95 nm. These fibers are piled together to form an opaque ES-PHB film (Figure 1b). Figure S2a,b shows the cross-sectional view of the Cast-PHB film. Clearly, the film has a nonfibrous structure. It exhibits high crystallinity (Figure S2c) and negligible optical transmittance (Figure 1b).

After the ES-PHB film was treated with a high pressure, a transparent HP-ESPHB film was acquired (Figures S3 and S4). As shown in Figure 1d, the transparent film has a flat surface, and previous pores between these fibers even disappeared. Simultaneously, because the ES-PHB film is squeezed violently under pressure, it loses the original fibrous morphology and the fibers fuse into a whole. However, the interior structure of the HP-ESPHB film is different from that of the Cast-PHB film. Here, Figure 1e,f exhibits the morphology of the cross section of the HP-ESPHB film. Apparently, there is still a large number of intact fiber structures in the transparent film, and these PHB fibers are packed together closely.

The transparency mechanism of the HP-ESPHB fibrous film is worth further discussion and study. When light propagates in the material, the light absorption, reflection, and scattering will cause light loss. While the light loss is large, the material becomes opaque. Because of the wide band gap of PHB, it is difficult for the photo energy of visible light to excite the transition of electrons from valence band to conduction band, and the light absorption caused by PHB is very small.

When light enters the material from the air, there is reflection at the interface between the air and the material. This will cause light loss and reduce light transmittance. Figure 1g shows the difference in light reflection in ES-PHB and HP-ESPHB films. For the ES-PHB film, because there are many voids in the electrospun film, numerous air−fiber interfaces are formed. The reflection of light at the interfaces depends on the refractive index of the two mediums, and the reflection coefficients follow[65]

$$R = \left(\frac{n_{21} - 1}{n_{21} + 1}\right)^2 \tag{2}$$

$$n_{21} = \frac{n_2}{n_1} \tag{3}$$

where R is the reflection coefficient and n_{21} is the relative refractive index of PHB fiber to air. n_1 and n_2 are the refractive indices of air and fiber, respectively. It is known that the greater the difference in refractive index between the two mediums, the greater is the reflection coefficient of light at the interface. Because of the large difference in refractive index of air and PHB, R of the ES-PHB fiber is large. This can cause much reflection loss of light. However, for the HP-ESPHB film, it is squeezed by a strong force, and these pores in ES-PHB film disappear. The air−fiber interfaces are replaced by the fiber−fiber interfaces. Since these PHB fibers have a similar refractive index, the relative refractive index at the interface between the PHB fibers can be approximated as 1. Consequently, the reflection coefficient at the interface is close to 0. This results in very small light loss.

Scattering in the material also has a lot of influence on the light transmittance. When the scattering effect is very strong, almost no light can pass through the medium and the material loses transparency. In general, crystalline polymers are polycrystalline systems with random grain orientation, so light is easily scattered in crystalline polymers. Consequently, most crystalline polymers are translucent or opaque. There is a positive relation between the crystallinity, crystalline size, and light scattering. However, Figure 1h,i exhibits that the HP-ESPHB film has higher crystallinity than the ES-PHB film, and they have similar crystalline structures. Additionally, the HP-ESPHB film has a larger crystalline size according to the full width at half-maximum (fwhm) of the diffraction peaks (Figure 1i). Higher crystallinity and larger crystalline size are detrimental to the light transmittance of the material, so the small light scattering in HP-ESPHB fibers should be ascribed to other factors.

In fact, the arrangement direction of crystals also affects the scattering of the material.[66,67] The XRD pole figure technique is an effective technology to study the crystalline orientation.[68,69] By analyzing the polar diagram, the order of grain orientation can be evaluated. Here, Figure 1j,k shows the pole figures of ES-PHB and HP-ESPHB. The maximum pole density of ES-PHB and HP-ESPHB is 7.2 mrd (multiple of random distribution) and 26.13 mrd, respectively. The degree of crystal orientation is positively correlated to the pole density. This means that an increase in the number of grains with specific orientations will lead to an increase in the pole density. When the order of the crystals is obvious, the pole density correspondingly increases. Therefore, the pole density can be used to evaluate the strength of the crystal orientation. Apparently, the crystals within HP-ESPHB have a more obvious orientation. When the orientation direction of the crystals is parallel to the direction of light, it can cause less hindrance to the light propagation and reduce the scattering and reflection. The loss of light propagation in the material is reduced, and the light transmittance is enhanced. Hence, it is possible that the crystal orientation in the HP-ESPHB is consistent with the propagation direction of the light. This reduces the scattering of light and improves the light transmittance of the PHB fibrous film.

For polymeric and composite transparent films, haze provides a direct and widely accepted metric of forward scattering in the materials.[53] The haze factor (H_T) can be calculated using the following equation[53]

$$H_T = \frac{T_{diff}(\lambda)}{T_{tot}(\lambda)} \tag{4}$$

where T_{tot} is the total transmittance of the film; T_{diff} is the diffuse transmittance of the film; and λ is the wavelength of the optical wave. Figure S10a,b and Table S2 show a comparison of the total transmittance and haze of the ES-PHB film (thickness: ∼22 μm) with a HP-ESPHB film (thickness: ∼84 μm). The HP-ESPHB film is nearly 4 times thicker than the ES-PHB film, yet the ES-PHB film exhibits significantly lower optical transmittance and a significantly higher haze. Notably,

Downloaded from pubs.acs.org/ascecg/article-pdf/14/1/198/6380243/sc5c09169.pdf by SOUTHWEST JIAOTONG UNIV user on 07 November 2026

https://doi.org/10.1021/acssuschemeng.5c09169
ACS Sustainable Chem. Eng. 2026, 14, 198−208

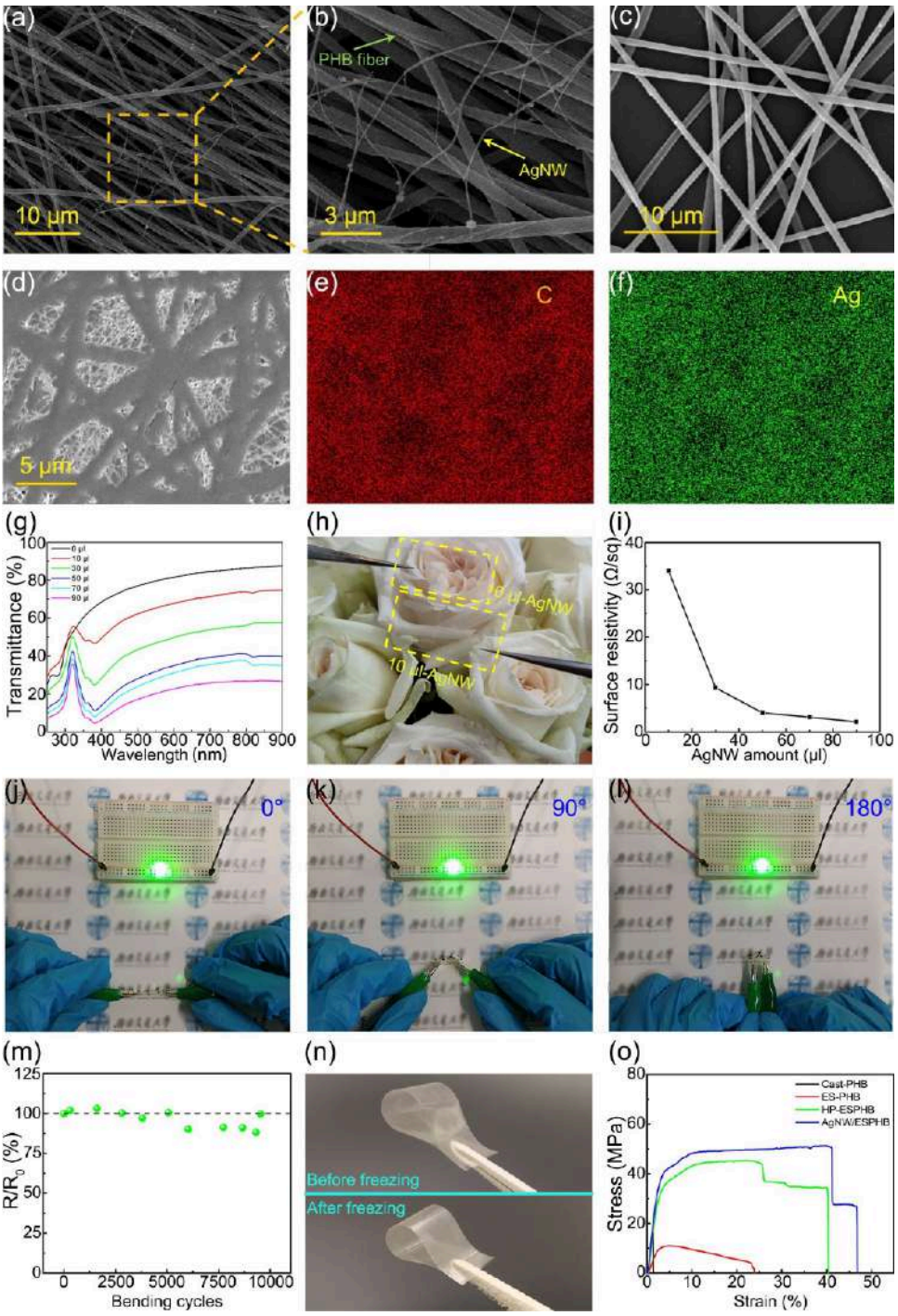


Figure 2. (a, b) SEM of AgNWs dispersed on the ES-PHB fibrous film by vacuum filtration before high-pressure treatment. (c) SEM of PI film covered by electrospun PHB fibers. (d–f) SEM (d) and EDS (e, f) of the AgNW/ESPHB fibrous film after high-pressure treatment. (g) Light transmittance of different AgNW/ESPHB fibrous films. The thickness of films is ~20 μm. (h) Digital picture of pristine HP-ESPHB and AgNW/ESPHB films. (i) Surface resistance of different AgNW/ESPHB fibrous films. (j–l) Bending properties. (m) Bending stability. (n) Flexibility at room temperature (top) and at liquid nitrogen temperature (bottom), respectively. (o) Tensile properties.

at 550 nm wavelength, the haze factor of the ES-PHB film is more than 4 times higher than that of the HP-ESPHB film. The ultrahigh haze renders the ES-PHB film white. In contrast, the HP-ESPHB film became highly transparent with a relatively low optical haze. As shown in Figure S10c, even when the HP-ESPHB film is placed 10 cm above the black board, the white grid remains clearly visible. This conclusively demonstrates that light scattering in the HP-ESPHB film was substantially reduced.

We further combined the conductive AgNW with the transparent HP-ESPHB film to prepare a transparent and conductive material (Figure S5). Figure 2a,b shows the AgNW dispersed on the ES-PHB film using filtration. The length of the AgNW is approximately 10–20 μm, and these nanowires are uniformly dispersed on the surface of the ES-PHB film.

https://doi.org/10.1021/acssuschemeng.5c09169
ACS Sustainable Chem. Eng. 2026, 14, 198–208

Downloaded from pubs.acs.org/ascecg/article-pdf/14/1/198/6380243/sc5c09169.pdf by SOUTHWEST JIAOTONG UNIV user on 07 November 2026

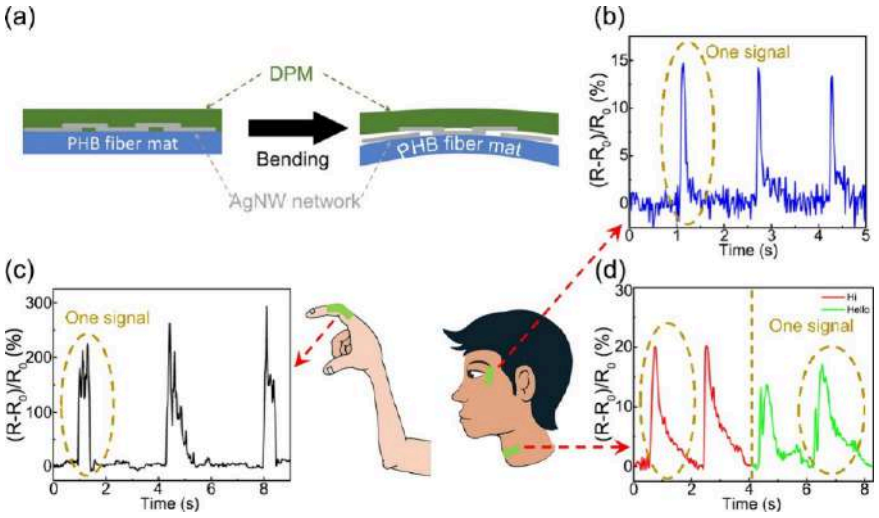


Figure 3. (a) Schematic diagram of the operation principle of the sensor. (b–d) The signal from the sensor when the volunteer's eyelid blinks (b), finger bends (c), and throat vocal cord vibrates (d).

Simultaneously, a layer of ultrathin PHB fibrous film was deposited on a polyamide (PI) membrane (Figure S5). Figure 2c exhibits these PHB fibers on the PI membrane, and the thickness of the ultrathin PHB film is only a few microns. In high-pressure treatment, the ultrathin film was transferred onto the AgNW network. It played an important role in stabilizing and protecting the conductive network. Figure 2d exhibits the surface morphology of the conductive AgNW/ESPHB film. The PHB fibers, originally deposited on the PI membrane, were significantly deformed under high pressure. These "flat" PHB fibers, like a large net, are on the conductive AgNW network and fix these nanowires on the PHB fibrous matrix. Figure 2e,f shows the distribution of C and Ag elements in the surface of AgNW/ESPHB film. Evidently, these two elements are evenly distributed in this view. This means that the AgNW is uniformly distributed on the PHB fibrous matrix and forms a conductive network that does endow the conductivity of the composite film (Figure 2d).

Importantly, the amount of AgNWs has a significant effect on the light transmittance and electrical conductivity of the composite film. Here, we use the volume of the AgNW aqueous solution to represent the amount of nanowire. Figure 2g exhibits the light transmittance of different AgNW/ESPHB films. The transmittance of HP-ESPHB is about 85% at 750 nm. When the volume of the AgNW solution is 10 μL, the transmittance of the composite film decreases to approximately 73% at 750 nm, but the AgNW/ESPHB-based film still has good transparency (Figure 2h). At the same time, as the volume of AgNW solution increases, the transparency of the film decreases. However, the conductivity of AgNW/ESPHB film augments with the increase of the volume of the AgNW solution. As shown in Figure 2i, when the volume of AgNW solution is 10 and 90 μL, respectively, the surface resistance of the AgNW/ESPHB film is 34 and 2.1 Ω/sq, respectively.

Because the transparent composite film consists of a lot of soft fibers, it has great mechanical properties. As shown in Figure 2j–l, the conductive AgNW/ESPHB film is used as a wire to light an LED. Although the bending angle of the film is increasing gradually, the brightness of the LED does not show obvious attenuation. This result indicates that the conductive film has good structural stability. Furthermore, the durability of the flexible AgNW/ESPHB film was evaluated. Figure 2m shows the change in resistance of the composite film during ~10 000 bending cycles. Apparently, the resistance did not change significantly in the bending test. This means that the film has good durability. Additionally, Figure 2n shows the flexibility of the conductive film at room temperature and ultralow temperature. The film could be easily folded in half at room temperature. On the premise of keeping the bending state, even if the film was placed in liquid nitrogen, it did not suffer obvious structural damage. Figure 2o shows a comparison of the tensile properties of the Cast-PHB, ES-PHB, HP-ESPHB, and AgNW/ESPHB films. For the AgNW/ESPHB-based film, elastic deformation and stress yield occur in the initial stage of drawing. The tensile strength and elongation at break are apparently higher than those of the Cast-PHB, ES-PHB, and HP-ESPHB films. It can be observed that the tensile performance of the HP-ESPHB film shows a significant improvement compared to those of the Cast-PHB and ES-PHB films. This indicates that the enhanced tensile performance of the AgNW/ESPHB film is primarily ascribed to the transparent PHB fibrous substrate. First, the substrate has a higher degree of crystallinity. In general, the polymers with high crystallinity have more integrity of crystals, and the interaction between crystals is enhanced. These are beneficial for mechanical performances. Second, the tight structure of the transparent fibrous substrate may contribute to the mechanical properties of the composite film. When the AgNW/ESPHB film is stretched, the sliding of fibers needs to overcome a large internal friction. Moreover, we note that the tensile performance of the AgNW/ESPHB-based film is moderately superior to that of the HP-ESPHB-based film. This suggests that the reinforcing effect of AgNW also makes a contribution to improving the tensile properties of the AgNW/ESPHB-based composite film.[53,70]

As shown in Table S1 and Figure S6, although the light transmittance of the AgNW/ESPHB-based composite film is slightly lower than that of other degradable transparent conductive materials, it has good electrical conductivity and tensile strength. Considering the large thickness of the AgNW/ESPHB-based composite film, the light transmittance of the film can be further improved by optimizing the preparation process. We also note the AgNW/ESPHB-based film exhibits a lower figure of merit (FoM) compared to the commercial

Downloaded from pubs.acs.org/ascecg/article-pdf/14/1/198/6380243/sc5c09169.pdf by SOUTHWEST JIAOTONG UNIV user on 07 November 2026

https://doi.org/10.1021/acssuschemeng.5c09169
ACS Sustainable Chem. Eng. 2026, 14, 198–208

ITO-based film (Figure S10a,b and Table S2). Nevertheless, owing to its excellent biocompatibility and degradability, the AgNW/ESPHB film is a highly promising eco-friendly alternative material for bioelectronic applications. The FoM of the PHB-based transparent conductive film can be enhanced by optimizing the conductive layer in future research, such as using conductive metal nanomeshes or cross-aligned AgNW networks. In summary, the fibrous PHB-based flexible transparent conductive film has good comprehensive performance. This means that the composite material has broad prospects in eco-friendly flexible transient bioelectronics.

Here, a resistive sensor was fabricated with the AgNW/ESPHB-based film (Figure S7). The bending modulus of the degradable packaging material (DPM) is different from that of HP-ESPHB. Thus, when the sensor is bent, the deformations of the two materials are different. As shown in Figure 3a, it entails a tiny gap between the DPM and the AgNW/ESPHB. Because some AgNWs are wrapped by the DPM, they are pulled up. This results in a decrease in the number of contact points in the AgNW network and an increase in the resistance of the sensor. When the deformation of the sensor is recovered, the gap disappears. The connection of these conductive nanowires is restored, and the resistance of the sensor decreases. Figure S11a shows the relative resistance change of the AgNW/ESPHB sensor at different bending frequencies, and the response time is 0.26 s (Figure S11b). The durability of the sensor is also measured: after over 800 bending cycles, the response signals of the sensor remain stable (Figure S11c). Gauge Factor (GF) is one of the indicators of the sensitivity of a resistive sensor, which is defined as[54]

$$\mathrm{GF} = \frac{(R - R_0)/R_0}{\varepsilon} \tag{5}$$

where R_0 represents the initial resistance; R is the resistance under a strain; and ε is the corresponding applied strain. Despite its low stretchability, the sensor achieves a high GF of 33.06 (Figure S11d).Therefore, this device can be used in behavior monitoring. As shown in Figure 3b,c, the sensor can perceive the motion of finger bending and eyelid blinking. Every bend of the finger or every blink of the eyelid induces a resistance change of the sensor regularly. Additionally, this device has much potential for speech recognition. While the sensor is tightly attached to the throat, the volunteer's sound will drive it to produce characteristic signals. For example, when the volunteer says "Hello" and "Hi" separately, the difference occurs in the number of signal peaks (Figure 3d).

Fluorescent CQD/CNC/PHB-based piezoelectric nanofibers (Figure S8a) can be used to manufacture PENG with green light-emitting function.[71] The commercial ITO has good transparency and conductivity and usually serves as a transparent electrode. However, its transmittance to ultraviolet light is low, and it cannot be used as the electrode for green light-emitting piezoelectric devices (Figure S8b). Because the AgNW/ESPHB film has excellent conductivity and high transmittance to ultraviolet light (Figure 2g), it is expected to be used as a TDE of the multifunctional PENG. Figure S9 exhibits the structure of the PENG consisting of DPM, AgNW/ESPHB film, and CQD/CNC/PHB fibers. In the test, two pieces of copper foil were extended from the PENG to transmit electrical signals (Figure 4a). As shown in Figure 4b, ultraviolet light passes through DPM and AgNW/ESPHB film and excites the CQD/CNC/PHB fiber to emit green fluorescence. The direction of the current signals generated

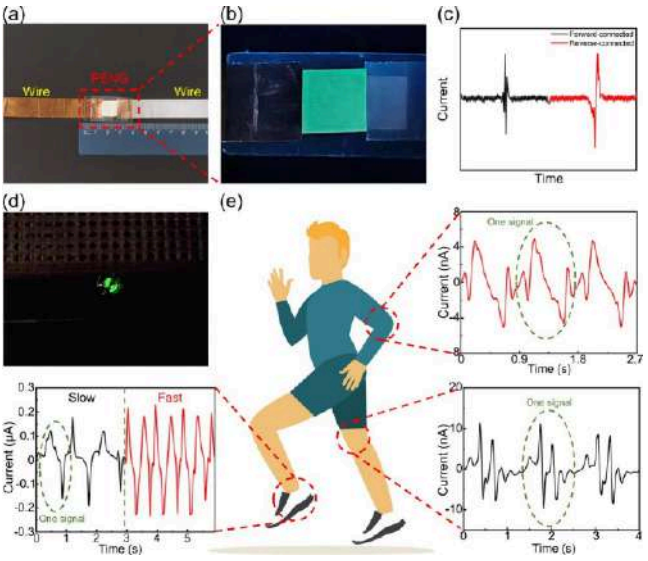


Figure 4. (a) Digital picture of the transient PENG for piezoelectric testing. (b) Under UV excitation, transient PENG emits green light. (c) Switching polarity test. (d) Transient PENG supplies energy for the LED. (e) Transient PENG for human behavioral monitoring.

by the PENG is reversed in the switching-polarity test (Figure 4c). This confirms the output signals truly come from the direct piezo responses of the fully biobased PENG device. Additionally, the PENG serves as a reliable power supply to maintain the operation of a commercial LED (Figure 4d). Because this device responds to mechanical stimuli, it can be used as a self-powered flexible sensor for real-time monitoring. As shown in Figure 4e, the sensor exhibits the motion of different human joints and the state of a human walking through the generated electrical signals. This result indicates it has great application prospects in motion monitoring, behavioral perception, etc.

Since the PENG is composed of various degradable materials, it is possible to attain complete degradation. In particular, PHB contains hydrolyzable ester bonds in its main chain structure. This makes it susceptible to both abiotic and biotic hydrolysis.[72−77] In the abiotic hydrolysis degradation process, PHB is first broken down into oligomers/fragments and eventually converted into crotonic acid and 3-hydroxybutyric acid.[72,73] Increasing temperature and/or using a more alkaline hydrolysis medium can in general enhance the hydrolytic degradation of PHB.[72,73] The degradation of PHB in a biotic compost environment is an enzymatic process.[74−77] It begins with an initial biomediated hydrolysis by microorganism secreted PHB depolymerases.[74−77] In the initial hydrolysis, PHB degrades into oligomers, dimers, and monomers.[74−77] These degradation products are further metabolized by microorganisms.[74−77] In aerobic environments, the final metabolites are microbial biomass, carbon dioxide, and water.[74−77] Under anaerobic conditions, methane is also produced alongside carbon dioxide.[74−77] Compost environmental conditions and microbial activity are key factors affecting the biodegradation efficiency of PHB.[74−77]

Here, the degradation of the PENG was conducted in an abiotic alkaline solution and biotic compost environment, respectively. Figure 5a exhibits the change of the morphology of the PENG in an aqueous solution of pH 12. When the degradation time reached 43 days, the DPM lost its transparency and became white and opaque. Additionally,

Downloaded from pubs.acs.org/ascecg/article-pdf/14/1/198/6380243/sc5c09169.pdf by SOUTHWEST JIAOTONG UNIV user on 07 November 2026

https://doi.org/10.1021/acssuschemeng.5c09169
ACS Sustainable Chem. Eng. 2026, 14, 198−208

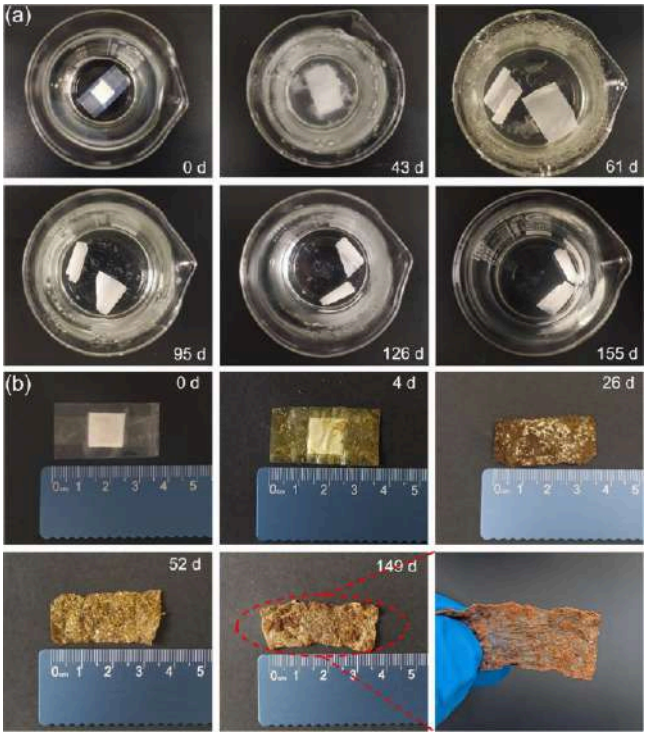


Figure 5. Hydrolytic degradation (a) and composting degradation (b) of the transient PENG device.

the device was destroyed and the interior fibrous film entered the hydrolysate. The piezoelectric film lost its original form and became a white flocculent substance. Then, these flocculent substances almost disappeared within 61 days. At the same time, the AgNW/ESPHB electrode broke into a number of fragments of different sizes. When the degradation time was more than 95 days, the size and number of fragments of the AgNW/ESPHB film further decreased. At 155 days, there was only a little debris of the conductive film and two pieces of white DPM. Figure 5b presents the degradation of PENG in the composting test. With the extension of composting time, the deformation of this device became more obvious. Simultaneously, the mechanical strength of the device gradually decreased. These phenomena suggest the degradation of PENG. At 149 days, the piezoelectric fibrous film and AgNW/ESPHB-based electrode in the degradable PENG seemed to have completely disappeared, leaving only the transparent encapsulation materials. These degradation experiments manifest that the transient PENG can be degraded in various environments. As a result, this could reduce the disposal costs of discarded devices and reduce the threat to public health.

CONCLUSIONS

Here, a combination of electrospinning and high-pressure molding techniques was employed to produce a transparent PHB film that contained intact fiber structures. At an appropriate temperature, applying a high pressure to the ES-PHB reduced the fiber−air interfaces and consequently minimized the light reflection loss. Simultaneously, the crystals within the PHB fiber aligned parallel to the incident light direction, resulting in reduced light scattering. These combined effects significantly enhanced the transparency of the PHB fibrous film, and a transmittance of 85% at 750 nm was achieved for the HP-ESPHB film. Subsequently, a transparent, conductive AgNW/ESPHB-based composite film was developed by using the HP-ESPHB film. This composite material exhibited both good electrical conductivity and high light transmittance alongside robust mechanical properties. It has great potential for applications in versatile transient electronic devices. For example, the AgNW/ESPHB-based film could be used in a degradable resistive sensor. Additionally, the AgNW/ESPHB-based conductive film could serve as a transparent degradable electrode for multifunctional biobased PENGs. This innovation allowed for the first creation of a fully degradable, environmentally friendly, luminescent, and self-powered bioelectric device. This research provides an effective but simple method for the modification of biological materials and offers valuable insights into the relationship between condensed matter structure and material properties. Furthermore, the AgNW/ESPHB-based composite material opens up new possibilities for further advancements in transient electronics.

ASSOCIATED CONTENT

Supporting Information

The Supporting Information is available free of charge at https://pubs.acs.org/doi/10.1021/acssuschemeng.5c09169.

Figures S1−S11: Fiber diameter distribution of ES-PHB fibers; Cross-sectional SEM images and DSC data of Cast-PHB film; Preparation of transparent HP-PHB film; Light transmittance of HP-ESPHB fibrous films prepared under different conditions; Preparation of transparent AgNW/ESPHB film; A diagram for the performance comparison of different environmental-friendly, degradable transparent conductive materials; Schematic diagram and digital picture of AgNW/ESPHB-based resistive sensor; CQD/CNC/PHB fibrous film and the piezoelectric device assembled using DPM, flexible ITO, and CQD/CNC/PHB fibrous film under natural light and ultraviolet light, respectively; Schematic diagram of the composite structure of the fully biobased, transient PENG device; Optical properties of PHB-based materials and ITO-PET film; durability of the AgNW/ESPHB-based resistive sensor; Tables S1−S2: A comparison of different environmental-friendly, degradable transparent conductive materials; the transmittance, haze factor, square resistance, FoM, thickness, and degradability of various PHB-based materials and ITO-PET film (PDF)

AUTHOR INFORMATION

Corresponding Authors

Weiqing Yang − *Research Institute of Frontier Science, Southwest Jiaotong University, Chengdu, Sichuan 610031, China;* orcid.org/0000-0001-8828-9862; Email: wqyang@swjtu.edu.cn

#Jun Lu − *School of Chemistry, Southwest Jiaotong University, Chengdu, Sichuan 610031, China;* orcid.org/0000-0002-0606-9565; Email: junluprc@hotmail.com

Authors

Chuanfeng Wang − *School of Chemistry and Key Laboratory of Advanced Technologies of Materials, Ministry of Education, School of Materials Science and Engineering, Southwest Jiaotong University, Chengdu, Sichuan 610031,*

Downloaded from pubs.acs.org/ascecg/article-pdf/14/1/198/6380243/sc5c09169.pdf by SOUTHWEST JIAOTONG UNIV user on 07 November 2026

China; CSSC Jiujiang Marine Equipment (Group) Co., Ltd., Jiujiang, Jiangxi 332005, China

Chu Pan − *School of Chemistry, Southwest Jiaotong University, Chengdu, Sichuan 610031, China*

Zhu Liu − *Key Laboratory of Advanced Technologies of Materials, Ministry of Education, School of Materials Science and Engineering, Southwest Jiaotong University, Chengdu, Sichuan 610031, China*

Liang Lu − *Key Laboratory of Advanced Technologies of Materials, Ministry of Education, School of Materials Science and Engineering, Southwest Jiaotong University, Chengdu, Sichuan 610031, China*

Yu Lai − *Key Laboratory of Advanced Technologies of Materials, Ministry of Education, School of Materials Science and Engineering, Southwest Jiaotong University, Chengdu, Sichuan 610031, China*

Juan Li − *School of Chemistry, Southwest Jiaotong University, Chengdu, Sichuan 610031, China*

Zhipei Xia − *School of Chemistry, Southwest Jiaotong University, Chengdu, Sichuan 610031, China*

Complete contact information is available at: https://pubs.acs.org/10.1021/acssuschemeng.5c09169

Author Contributions

[▽]C.W. and C.P. contributed equally to this work. J. Lu and C.W. conceived the idea. J. Lu initiated the study. C.W., C.P., Z.L., L.L., Y.L., J. Li, and Z.X. carried out the sample preparation and characterization. J. Lu and W.Y. organized the entire research. C.W., J. Lu, and W.Y. analyzed and interpreted the data and wrote the manuscript with the assistance of all other coauthors. All authors discussed the results and commented on the manuscript.

Notes

The authors declare no competing financial interest.

[#]Other used names are Jun Lv and Jun Lyu.

■ ACKNOWLEDGMENTS

This work was financially supported by National Natural Science Foundation of China (No. 52073237), State Key Laboratory of Molecular Engineering of Polymers (Fudan University) (No. K2020-09), and Young Scientific and Technological Innovation Research Team Funds of Sichuan Province (No. 20CXTD0106). The authors would like to thank the Analysis and Testing Center of Southwest Jiaotong University.

■ REFERENCES

(1) Grant, K.; Goldizen, F. C.; Sly, P. D.; Brune, M.-N.; Neira, M.; van den Berg, M.; Norman, R. E. Health consequences of exposure to e-waste: A systematic review. *Lancet Glob. Health* **2013**, *1* (6), e350−e361.

(2) Rene, E. R.; Sethurajan, M.; Kumar Ponnusamy, V.; Kumar, G.; Bao Dung, T. N.; Brindhadevi, K.; Pugazhendhi, A. Electronic waste generation, recycling and resource recovery: Technological perspectives and trends. *J. Hazard. Mater.* **2021**, *416*, No. 125664.

(3) Shen, C. Y.; Jia, L.; Yang, Y. Fully medical waste-based triboelectric nanogenerator for energy harvesting and intelligent human motion sensing. *ACS Sustain. Chem. Eng.* **2024**, *12* (38), 14141−14152.

(4) Liu, Q. H.; Li, J. H.; Mu, L. H.; He, J. M.; Liu, H.; Zhu, M. L.; Feng, P.; Zhang, R. Z.; Sun, C. L.; Qu, M. N. Loofah-derived superhydrophobic and flame-retardant nanofiber paper for sustainable all-weather piezoresistive sensing monitoring and green triboelectric energy harvesting. *ACS Sustain. Chem. Eng.* **2025**, *13* (29), 11591−11606.

(5) Shim, J.-S.; Rogers, J. A.; Kang, S.-K. Physically transient electronic materials and devices. *Mater. Sci. Eng. R* **2021**, *145*, No. 100624.

(6) Feig, V. R.; Tran, H.; Bao, Z. Biodegradable polymeric materials in degradable electronic devices. *ACS Central Sci.* **2018**, *4* (3), 337−348.

(7) Hu, Z. Y.; Guo, H. X.; An, D. Q.; Wu, M. Z.; Kaura, A.; Oh, H.; Wang, Y.; Zhao, M. J.; Li, S.; Yang, Q. S.; Ji, X. D.; Li, S. P.; Wang, B.; Yoo, D.; Tran, P.; Ghoreishi-Haack, N.; Kozorovitskiy, Y.; Huang, Y. G.; Li, R.; Rogers, J. A. Bioresorbable multilayer organic-inorganic films for bioelectronic systems. *Adv. Mater.* **2024**, *36* (19), No. 2309421.

(8) Jung, H.; Seo, H.; Sim, G.; Avila, R.; Nair, M.; Kim, B.; Choi, Y. Bioresorbable polymers for electronic medicine. *Cell. Rep. Phys. Sci.* **2024**, *5* (8), No. 102099.

(9) Hu, C.; Wang, L.; Liu, S. B.; Sheng, X.; Yin, L. Recent development of implantable chemical sensors utilizing flexible and biodegradable materials for biomedical applications. *ACS Nano* **2024**, *18* (5), 3969−3995.

(10) Sandhu, S.; Dahiya, R. End-of-life usefulness of degradation by products from transient electronics. *npj Flex. Electron.* **2025**, *9* (1), 37.

(11) Chen, L.; Liang, H. K.; Liu, P.; Liu, C. H.; Feng, B.; Shu, Z. W.; Chen, Y. Q.; Dong, X. Q.; Xie, J. F.; Ji, M.; Duan, H. G. Sustainable lithography paradigm enabled by mechanically peelable resists. *Adv. Mater.* **2025**, *37* (3), No. 2410978.

(12) Ko, J.; Kim, S.; Kim, D.; Lim, T.; Jin, S.; Jeong, Y.; Joo, Y.; Cho, S. A. Biodegradable radical polymer enables high-performance, physically transient organic memory. *Angew. Chem., Int. Ed.* **2025**, *64* (27), No. e202422826.

(13) Wu, T.; Xie, F. F.; Guo, X. X.; Zhang, E. H.; Lu, Y. A wood cell wall-derived triboelectric nanogenerator for energy harvesting and multifunctional sensing. *ACS Sustain. Chem. Eng.* **2025**, *13* (31), 12594−12604.

(14) Shi, J. Y.; Li, P. J.; Kim, S.; Tian, B. Z. Implantable bioelectronic devices for photoelectrochemical and electrochemical modulation of cells and tissues. *Nat. Rev. Bioeng.* **2025**, *3* (6), 485−504.

(15) Madsen, K. E.; Flavin, M. T.; Rogers, J. A. Materials advances for distributed environmental sensor networks at scale. *Nat. Rev. Mater.* **2025**, DOI: 10.1038/s41578-025-00838-7.

(16) Li, Q. S.; Ji, S. B.; Li, G. L.; Liu, Z. Y.; Chen, X. D. Engineering silkworm silk for mechanically and biologically compliant skin electronics. *Acc. Mater. Res.* **2025**, *6*, 1177.

(17) Nair, N. M.; Zumeit, A.; Dahiya, R. Transparent and transient flexible electronics. *Adv. Sci.* **2025**, *12* (31), No. e05133.

(18) Wager, J. F. Transparent electronics. *Science* **2003**, *300* (5623), 1245−1246.

(19) Kim, K.; Park, Y. G.; Hyun, B. G.; Choi, M.; Park, J. U. Recent advances in transparent electronics with stretchable forms. *Adv. Mater.* **2019**, *31* (20), No. 1804690.

(20) Luo, C. S.; Wan, P.; Yang, H.; Shah, S. A. A.; Chen, X. Healable transparent electronic devices. *Adv. Funct. Mater.* **2017**, *27* (23), No. 1606339.

(21) Wang, T.; Guo, Y.; Wan, P.; Zhang, H.; Chen, X.; Sun, X. Flexible transparent electronic gas sensors. *Small* **2016**, *12* (28), 3748−3756.

(22) Service, R. F. See-through solar cells could power offices. *Science* **2018**, *360* (6396), 1386−1386.

(23) Lee, S.; Kim, S.-W.; Ghidelli, M.; An, H. S.; Jang, J.; Bassi, A. L.; Lee, S.-Y.; Park, J.-U. Integration of transparent supercapacitors and electrodes using nanostructured metallic glass films for wirelessly rechargeable, skin heat patches. *Nano Lett.* **2020**, *20* (7), 4872−4881.

(24) Li, W.; Akhter, Z.; Vaseem, M.; Shamim, A. Optically transparent and flexible radio frequency electronics through printing technologies. *Adv. Mater. Technol. - US* **2022**, *7* (6), No. 2101277.

(25) Althumayri, M.; Das, R.; Banavath, R.; Beker, L.; Achim, A. M.; Koydemir, H. C. Recent advances in transparent electrodes and their

Downloaded from pubs.acs.org/ascecg/article-pdf/14/1/198/6380243/sc5c09169.pdf by SOUTHWEST JIAOTONG UNIV user on 07 November 2026

multimodal sensing applications. *Adv. Sci.* **2024**, *11* (38), No. 2405099.
(26) Ju, Z. S.; Chen, Y. S.; Li, P.; Ma, J. G.; Xu, H. Y.; Liu, Y. C.; Samori, P. Dressing AgNWs with MXenes nanosheets: Transparent printed electrodes combining high-conductivity and tunable work function for high-performance opto-electronics. *Adv. Mater.* **2024**, *36* (48), No. 2412512.
(27) Wang, F.; Wang, K. K.; Chang, Z. Y.; Liang, H. R.; Jiang, Q. Y.; Xi, A. K.; Zhao, Y. L.; Zhao, S. M.; Leu, K. X.; Wu, X. K.; Li, R.; Huang, Y.; Zhang, Y. Y.; Zhang, R. F. Highly transparent and transferable ultralong carbon nanotube networks for transparent wearable electronics. *ACS Nano* **2024**, *18* (48), 33245−33255.
(28) Lee, E. K.; Baruah, R. K.; Bhamra, H.; Kim, Y.-J.; Yoo, H. Recent advances in electrode development for biomedical applications. *Biomed. Eng. Lett.* **2021**, *11* (2), 107−115.
(29) Hui, Z.; Zhang, L.; Ren, G.; Sun, G.; Yu, H. D.; Huang, W. Green flexible electronics: Natural materials, fabrication, and applications. *Adv. Mater.* **2023**, *35* (28), No. 2211202.
(30) Sannicolo, T.; Lagrange, M.; Cabos, A.; Celle, C.; Simonato, J. P.; Bellet, D. Metallic nanowire-based transparent electrodes for next generation flexible devices: A review. *Small* **2016**, *12* (44), 6052−6075.
(31) Won, P.; Park, J. J.; Lee, T.; Ha, I.; Han, S.; Choi, M.; Lee, J.; Hong, S.; Cho, K.-J.; Ko, S. H. Stretchable and transparent kirigami conductor of nanowire percolation network for electronic skin applications. *Nano Lett.* **2019**, *19* (9), 6087−6096.
(32) Han, J. H.; Kim, D.-h.; Jeong, E. G.; Lee, T.-W.; Lee, M. K.; Park, J. W.; Lee, H.; Choi, K. C. Highly conductive transparent and flexible electrodes including double-stacked thin metal films for transparent flexible electronics. *ACS Appl. Mater. Interfaces* **2017**, *9* (19), 16343−16350.
(33) Hanmandlu, C.; Chen, C.-Y.; Boopathi, K. M.; Lin, H.-W.; Lai, C.-S.; Chu, C.-W. Bifacial perovskite solar cells featuring semi-transparent electrodes. *ACS Appl. Mater. Interfaces* **2017**, *9* (38), 32635−32642.
(34) Lim, S.-H.; Seok, H.-J.; Kwak, M.-J.; Choi, D.-H.; Kim, S.-K.; Kim, D.-H.; Kim, H.-K. Semi-transparent perovskite solar cells with bidirectional transparent electrodes. *Nano Energy* **2021**, *82*, No. 105703.
(35) Sahu, D. R.; Lin, S.-Y.; Huang, J.-L. ZnO/Ag/ZnO multilayer films for the application of a very low resistance transparent electrode. *Appl. Surf. Sci.* **2006**, *252* (20), 7509−7514.
(36) Allhusen, J. S.; Conboy, J. C. Preparation and characterization of conductive and transparent ruthenium dioxide sol-gel films. *ACS Appl. Mater. Interfaces* **2013**, *5* (22), 11683−11691.
(37) Bob, B.; Machness, A.; Song, T.-B.; Zhou, H.; Chung, C.-H.; Yang, Y. Silver nanowires with semiconducting ligands for low-temperature transparent conductors. *Nano Res.* **2016**, *9* (2), 392−400.
(38) Akter, T.; Kim, W. S. Reversibly stretchable transparent conductive coatings of spray-deposited silver nanowires. *ACS Appl. Mater. Interfaces* **2012**, *4* (4), 1855−1859.
(39) Lee, J.; Lee, I.; Kim, T. S.; Lee, J. Y. Efficient welding of silver nanowire networks without post-processing. *Small* **2013**, *9* (17), 2887−2894.
(40) Tang, Q.; Zou, M.; Chang, L.; Guo, W. A super-flexible and transparent wood film/silver nanowire electrode for optical and capacitive dual-mode sensing wood-based electronic skin. *Chem. Eng. J.* **2022**, *430*, No. 132152.
(41) Gong, H.; Xu, Z.; Yang, Y.; Xu, Q.; Li, X.; Cheng, X.; Huang, Y.; Zhang, F.; Zhao, J.; Li, S.; Liu, X.; Huang, Q.; Guo, W. Transparent, stretchable and degradable protein electronic skin for biomechanical energy scavenging and wireless sensing. *Biosens. Bioelectron.* **2020**, *169*, No. 112567.
(42) Li, J.; Yang, H.; Huang, K.; Cao, S.; Ni, Y.; Huang, L.; Chen, L.; Ouyang, X. Conductive regenerated cellulose film as counter electrode for efficient dye-sensitized solar cells. *Cellulose* **2018**, *25* (9), 5113−5122.
(43) Yu, S.; Liu, Z.; Zhao, L.; Li, L. Degradable, ultra-flexible, transparent and conductive film made of assembling CuNWs on chitosan. *Opt. Mater.* **2022**, *123*, No. 111752.
(44) Pal, R. K.; Farghaly, A. A.; Wang, C.; Collinson, M. M.; Kundu, S. C.; Yadavalli, V. K. Conducting polymer-silk biocomposites for flexible and biodegradable electrochemical sensors. *Biosens. Bioelectron.* **2016**, *81*, 294−302.
(45) Zhang, C.; Nicolosi, V. Graphene and MXene-based transparent conductive electrodes and supercapacitors. *Energy Storage Mater.* **2019**, *16*, 102−125.
(46) Kim, S. J.; Cho, K. W.; Cho, H. R.; Wang, L.; Park, S. Y.; Lee, S. E.; Hyeon, T.; Lu, N.; Choi, S. H.; Kim, D. H. Stretchable and transparent biointerface using cell-sheet-graphene hybrid for electrophysiology and therapy of skeletal muscle. *Adv. Funct. Mater.* **2016**, *26* (19), 3207−3217.
(47) Zhuang, A.; Huang, X.; Fan, S.; Yao, X.; Zhu, B.; Zhang, Y. One-step approach to prepare transparent conductive regenerated silk fibroin/PEDOT:PSS films for electroactive cell culture. *ACS Appl. Mater. Interfaces* **2022**, *14* (1), 123−137.
(48) Xie, Y.; Lu, H.; Huang, J.; Xie, H. Natural materials for sustainable organic solar cells: status and challenge. *Adv. Funct. Mater.* **2023**, *33* (15), No. 2213910.
(49) Zhang, Y.; Ng, S.-W.; Lu, X.; Zheng, Z. Solution-processed transparent electrodes for emerging thin-film solar cells. *Chem. Rev.* **2020**, *120* (4), 2049−2122.
(50) Park, S.; Vosguerichian, M.; Bao, Z. A review of fabrication and applications of carbon nanotube film-based flexible electronics. *Nanoscale* **2013**, *5* (5), 1727−1752.
(51) Liu, J.; Guo, L.; Liu, Z.; Shen, Q.; Gao, X.; Zhang, Z.; Liu, X.; Cheng, K.; Du, Z. Improved thermal/chemical stability of flexible Ag NWs/chitosan composite electrode integrated by chemical welding and sequential protection for better PV performance. *Nanotechnology* **2021**, *32* (41), No. 415206.
(52) Luo, Y. T.; Zhou, Z. H.; Huang, Z. B.; Juang, J. Y.; Xu, L. Facile and versatile fabrication process for AgNW/GZO transparent composite electrodes for photovoltaic applications by atmospheric pressure plasma jet. *Appl. Surf. Sci.* **2023**, *635*, No. 157767.
(53) Chou, C. Y.; Hsu, L. C.; Lee, M. T.; Juang, J. Y. Enhanced flexural strength and optoelectrical properties of AgNW/GZO composite electrodes on flexible glass via atmospheric pressure plasma jet. *Mater. Design* **2025**, *258*, No. 114667.
(54) Chen, Y. Y.; Li, Y. L.; Zhang, Q.; Peng, T.; Yu, H. Z.; Shi, S. W. Recyclable and stable strain sensors based on semi-wrapped structure of silver nanowires in polyvinyl alcohol for human motion monitoring. *Macromol. Mater. Eng.* **2024**, *309* (11), No. 2400116.
(55) Raza, Z. A.; Abid, S.; Banat, I. M. Polyhydroxyalkanoates: Characteristics, production, recent developments and applications. *Int. Biodeter. Biodegr.* **2018**, *126*, 45−56.
(56) McAdam, B.; Brennan Fournet, M.; McDonald, P.; Mojicevic, M. Production of Polyhydroxybutyrate (PHB) and factors impacting its chemical and mechanical characteristics. *Polymers* **2020**, *12* (12), 2908.
(57) Bensalem, Z.; Chabane, H.; Ababsa, H. S.; Mekki, A.; Livi, S. Ionic liquids versus deep eutectic solvent: A tunable platform for the design of biopolymer blends. *ACS Sustainable Chem. Eng.* **2024**, *12* (3), 1309−1319.
(58) Zhang, H.; Ma, S. L.; Dou, X. T.; Chen, R.; Lu, H.; Chi, Z. Y.; Xue, S.; Li-Beisson, Y.; Kong, F. T. Harnessing algal peroxisomes for efficient poly hydroxybutyrate production. *ACS Sustainable Chem. Eng.* **2024**, *12* (8), 3312−3321.
(59) Armijo-Galdames, B. O.; Sadler, J. C. One-pot biosynthesis of acetone from waste poly(hydroxybutyrate). *ACS Sustainable Chem. Eng.* **2024**, *12* (20), 7748−7756.
(60) Rodrigues, J. A. F. R.; Parra, D. F.; Lugão, A. B. Crystallization on films of PHB/PEG blends. *J. Therm. Anal. Calorim.* **2005**, *79* (2), 379−381.
(61) Hsu, S.-H.; Hsieh, C.-T.; Sun, Y.-M. Synthesis and characterization of waterborne polyurethane containing poly (3-hydroxybuty-

Downloaded from pubs.acs.org/ascecg/article-pdf/14/1/198/6380243/sc5c09169.pdf by SOUTHWEST JIAOTONG UNIV user on 07 November 2026

https://doi.org/10.1021/acssuschemeng.5c09169
ACS Sustainable Chem. Eng. 2026, 14, 198−208

rate) as new biodegradable elastomers. *J. Mater. Chem. B* **2015**, *3* (47), 9089−9097.
(62) Shariatikia, F.; Sangroniz, L.; Olmedo-Martínez, J. L.; Pérez-Camargo, R. A.; González, A.; Lenzi, L.; Degli Esposti, M.; Morselli, D.; Fabbri, P.; Müller, A. J. Effect of biobased glycerol trilevulinate on the crystallization kinetics of biodegradable polyesters. *ACS Sustainable Chem. Eng.* **2025**, *13* (12), 4884−4896.
(63) Lin, Y.; Bilotti, E.; Bastiaansen, C. W. M.; Peijs, T. Transparent semi-crystalline polymeric materials and their nanocomposites: A review. *Polym. Eng. Sci.* **2020**, *60* (10), 2351−2376.
(64) Barham, P. J.; Keller, A.; Otun, E. L.; Holmes, P. A. Crystallization and morphology of a bacterial thermoplastic: poly-3-hydroxybutyrate. *J. Mater. Sci.* **1984**, *19* (9), 2781−2794.
(65) Xiao, Y.; Luo, H.; Tang, R.; Hou, J. Preparation and applications of electrospun optically transparent fibrous membrane. *Polymers* **2021**, *13* (4), 506.
(66) Mao, X.; Wang, S.; Shimai, S.; Guo, J. Transparent polycrystalline alumina ceramics with orientated optical axes. *J. Am. Ceram. Soc.* **2008**, *91* (10), 3431−3433.
(67) Yi, H.; Mao, X.; Zhou, G.; Chen, S.; Zou, X.; Wang, S.; Shimai, S. Crystal plane evolution of grain oriented alumina ceramics with high transparency. *Ceram. Int.* **2012**, *38* (7), 5557−5561.
(68) Su, C.; Shi, G.; Li, X.; Zhang, X.; Müller, A. J.; Wang, D.; Liu, G. Uniaxial and mixed orientations of poly (ethylene oxide) in nanoporous alumina studied by X-ray pole figure analysis. *Macromolecules* **2018**, *51* (23), 9484−9493.
(69) Widjonarko, N. Introduction to advanced X-ray diffraction techniques for polymeric thin films. *Coatings* **2016**, *6* (4), 54.
(70) Fu, J. J.; Han, X.; Su, X. M.; Huang, Z. L.; Yang, X. Q.; Luo, L.; Cao, X. Q.; Lang, J. P.; Gu, H. W. Flexible fluorine/nitrogen co-doped carbon electrodes with silver nanowire reinforcement enable ultra-long-cycling lithium-ion batteries. *Adv. Funct Mater.* **2025**, DOI: 10.1002/adfm.202514737.
(71) Wang, C.; Lu, L.; Liu, Z.; Lai, Y.; Li, J.; Xia, Z.; Cao, J.; Wang, X.; Lu, J.; Yang, W. Green carbon dots illuminate biogenic nanohybrids toward soft, piezo/photoactive, and physically transient nanogenerators. *ACS Sustain. Chem. Eng.* **2023**, *11* (40), 14646−14658.
(72) Yang, X.; Odelius, K.; Hakkarainen, M. Microwave-assisted reaction in green solvents recycles PHB to functional chemicals. *ACS Sustain. Chem. Eng.* **2014**, *2* (9), 2198−2203.
(73) Dhaini, A.; Hardouin-Duparc, V.; Alaaeddine, A.; Carpentier, J. F.; Guillaume, S. M. Recent advances in polyhydroxyalkanoates degradation and chemical recycling. *Prog. Polym. Sci.* **2024**, *149*, No. 101781.
(74) Gutierrez-Wing, M. T.; Stevens, B. E.; Theegala, C. S.; Negulescu, I. I.; Rusch, K. A. Aerobic biodegradation of polyhydroxybutyrate in compost. *Environ. Eng. Sci.* **2011**, *28* (7), 477−488.
(75) Dey, S.; Tribedi, P. Microbial functional diversity plays an important role in the degradation of polyhydroxybutyrate (PHB) in soil. *3 Biotech* **2018**, *8*, 171.
(76) Zhu, B. T.; Wang, D.; Wei, N. Enzyme discovery and engineering for sustainable plastic recycling. *Trends Biotechnol.* **2022**, *40* (1), 22−37.
(77) Paloyan, A.; Tadevosyan, M.; Ghevondyan, D.; Khoyetsyan, L.; Karapetyan, M.; Margaryan, A.; Antranikian, G.; Panosyan, H. Biodegradation of polyhydroxyalkanoates: current state and future prospects. *Front. Microbiol.* **2025**, *16*, No. 1542468.

Downloaded from pubs.acs.org/ascecg/article-pdf/14/1/198/6380243/sc5c09169.pdf by SOUTHWEST JIAOTONG UNIV user on 07 November 2026